Ocean Engineering 235 (2021) 109364

Contents lists available at ScienceDirect

Ocean Engineering

journal homepage: www.elsevier.com/locate/oceaneng

Structural reliability analysis of a seafastening structure for sea transport of heavy objects

Asle Natskår [a,b,*], Torgeir Moan [a,c]

[a] Department of Marine Technology, Norwegian University of Science and Technology (NTNU), Trondheim, Norway
[b] DNV, Marine Operations, Høvik, Norway
[c] Centre for Autonomous Marine Operations and Systems (AMOS) NTNU, Trondheim NO-7491, Norway

ARTICLE INFO

Keywords:
Marine operation
Sea transport
Structural reliability analysis
Structural capacity

ABSTRACT

This paper addresses the safety of marine operations related to a seafastening system for large-object transport. The aim is to present a structural reliability approach to accommodate the uncertainties affecting design checks. The probability of structural failure by use of design standards for assessing marine operations is studied using structural reliability analyses to shed light on the implicit reliability levels of such standards. A structural reliability model that includes the effect of uncertainty in weather forecasts is established. The reliability analyses show that the method to account for forecast uncertainty as defined in the standards compensates well for that uncertainty, and the failure probabilities in the case studies are between 10^{-4} and 10^{-3} per operation. A reliability model that includes the long-term statistical distribution of the environmental conditions is also established. This model is applicable for operations with a duration longer than three days and is used to study seasonal variations and the failure probability as a function of the duration of operations. The failure probability is calculated for execution in several months, showing the dependency on the time of the year and the duration of the operations. The failure probabilities are on the order of 10^{-4} per operation.

1. Introduction

In this paper, we study marine operations related to the sea transport of large and heavy objects. The consequences of failure can be severe, but an excessively conservative approach will increase costs. Therefore, an optimized safety level should be targeted. The uncertainties inherent in marine operations must thus be quantified in a reliability context to provide a rational basis for decision making. We will present a method to estimate the failure probability of seafastening and apply the method in studies related to sea transport on a towed barge. The study addresses both weather-restricted and weather-unrestricted transports.

Two different methods are used in this paper to calculate wave-induced barge motions. One approach is used for structural design when planning the transport, and another approach is applied in structural reliability analyses. The two different methods used are:

- The design check of the required capacity of the support points is based on the barge motions given in a design standard.
- The structural reliability analyses are based on barge motions as calculated by a 3D panel model.

The design check could have been based on motions calculated by the panel model instead of the standard method. The standard method was chosen to investigate the failure probability by the use of a simplified method for calculating barge motions as given by a design standard.

For weather-restricted operations (normally, operations with a duration of less than three days), the significant wave heights are based on weather forecasts, and the uncertainty in the weather forecasts of the significant wave height should be accounted for. The approach applied in this study is based on Natskår et al. (2015), where the uncertainty in the forecasts is included, as described in Section 2.7. Several other researchers have studied the uncertainty in predicted significant wave height, for example, De Girolamo et al. (2017). They studied the reliability of weather forecasts by analyzing the probability of correctly predicting a given threshold value of significant wave height. They studied the probability of "missed alarms", i.e., where the predicted significant wave height is below the threshold and the actual significant wave height is above the threshold, using different quantiles in the probability distribution of the forecast error. Gintautas and Sørensen (2016) developed a reliability-based method to estimate the number of weather windows and their length within a given time period. They

* Corresponding author at: Department of Marine Technology, Norwegian University of Science and Technology (NTNU), Trondheim, Norway.
E-mail address: asle.natskar@dnv.com (A. Natskår).

https://doi.org/10.1016/j.oceaneng.2021.109364
Received 3 October 2020; Received in revised form 16 June 2021; Accepted 19 June 2021
Available online 26 June 2021

concluded that the improved predictability of their approach increased the total length of the weather windows by 11% within the test period.

While we study marine operations through sea transportation, several other studies focused on the installation phase. Guachamin Acero et al. (2016) studied marine operations with regard to the assessment of the operational limits and the operability of marine operations related to the installation of an offshore wind turbine by a floating crane. They proposed a methodology where the operational limits were established in terms of maximum allowable sea states by taking into account the duration of subactivities. Other aspects of installation have also been studied, for example, by Guachamin Acero et al. (2015), who analyzed the crane installation of offshore wind turbines by calculating the motion in a sophisticated manner, including both the 1st- and 2nd-order responses of the crane barge and the lifted object. Sea transport and installation have in common that planning, e.g., accounting for the uncertainty in the predicted wave heights and calculating the vessel response, is vital for the control of the reliability level inherent in the operations.

Research has also been performed on the hull girder capacity in ship transport, e.g., by Shu and Moan (2011), who studied the interaction between the local load from the sea pressure and the hull girder bending of a bulk carrier. They found that the correlation between the wave-induced global and local loads had a negligible influence on the probability of failure and that it was reasonable to not consider the correlation between global and local wave loads in the structural reliability analysis. In this paper, we focus on the support structure rather than the bending of the hull girder of the transport vessel.

For weather-unrestricted operations (operations with durations of more than three days), the significant wave heights are based on long-term distributions, which in this study are estimated from hindcast data for the northern North Sea. The failure probability for a weather-unrestricted operation based on the long-term statistical data of the significant wave height is calculated assuming that the transport starts in several months throughout the year.

The reliability target level is based on existing structures because the target level should be consistent with the implied reliability level in current, accepted design practice. This study aims to provide an indication of this reliability level. The target reliability level could depend on, e.g., the consequences of failure, but that factor is not considered here.

This paper deals with the reliability of the seafastening system as affected by normal uncertainties due to the fundamental variability/uncertainty and lack of data. Human errors and omissions as well as organizational factors in the planning of the operation and design of the equipment and fabrication as well as during the execution of the marine operation might also cause failure. It is assumed herein that such errors are eliminated by suitable verification and control during the design, fabrication and operation. An organized risk management effort is normally used to manage the design process, and there should be continuous control and verification of the fabrication. Proper training of the personnel to be involved during the execution of the operation is also vital. In this paper, human errors are not considered, and the focus is on handling normal uncertainties in the framework of the structural reliability analysis.

In this paper, the planning and execution of marine operations are assumed to be performed according to the design standard *Marine Operations and Marine Warranty*, DNVGL-ST-N001 (2020).[1] The ISO standard for marine operations, i.e., ISO 19901-6 (2009), is also referred to.

[1] DNVGL-ST-N001 is not freely available. However, the requirements in that standard referred to in this paper are the same as in previous versions of the standard—i.e., DNV-OS-H101 and DNV-OS-H202, which are available for free on the internet.

2. Methodology

2.1. Organization of the paper

In this section (Section 2), some background information and a description of the method and the organization of the paper are given. In Section 3, case studies are presented, and the results are discussed in Section 4. In Section 5, conclusions and recommendations for further work are given. The paper is organized as follows:

- typical transport configurations (Section 2.3);
- identification of critical events and failure modes (Section 2.4);
- design of structural components (support structures) (Section 2.5);
- structural reliability analysis (Section 2.6);
- modeling of load effects (Section 2.7);
- modeling of resistance (Section 2.8);
- target reliability level for temporary phases (Section 2.9);
- case studies; calculating the failure probability as a function of the forecasted wave height, the season of the year, the duration of the operation, etc. (Section 3);
- results and discussion (Section 4); and
- conclusions and recommendations (Section 5).

2.2. Scope

For a structure to be transported—e.g., from its fabrication site to its final destination—there are several temporary phases, e.g., loading of the transport vessel, sea transport and discharge. Herein, we focus on the sea transport phase. The aim of the paper is to develop a reliability model for the structural capacity of cargo supports. Furthermore, we perform structural reliability analyses of the support structure and compare the implicit reliability level for various design conditions, e.g., for several forecasted significant wave heights, as a function of the duration of the operation, assuming that the operation occurs in various seasons of the year.

2.3. Typical transport configurations

Large and heavy objects can be transported on ships and barges. A transport barge loaded with a large object is shown in Fig. 1. The transported object is typically placed on preinstalled grillage beams, e.g., 2–5 m high, depending on the weight of the transported object, among other factors. The grillage beam configuration is shown in Fig. 2. The grillage beams transfer the vertical load from the transported object into the barge structure through the grillage beam end plates (wing plates), which are located on top of the bulkheads; see Fig. 3. The object is secured against movements in horizontal directions by the seafastening system (roll and pitch stoppers). In this paper, the vertical supports are the components of interest.

2.4. Critical events and failure modes

2.4.1. Critical events

In calm water and in moderate waves, the transport heads toward the destination independently of the wave and wind directions. When the environmental conditions exceed defined limits, the tow is assumed to head up against the waves, riding off the storm while trying to limit the barge roll motions. The relative wave direction for the barge is then head seas $\pm\theta$. The angle θ depends on the tug's ability to keep the towline tight and prevent yaw motions of the barge. The layout of the transported object and the barge also affects the relative wave direction. If the wind seas and swell directions are different, with the tow head up against the wind, the barge is exposed to waves from the side independent of θ. As a result, there could be a large relative wave angle. These effects are not investigated further within the present study, and the barge is therefore assumed to be exposed to beam

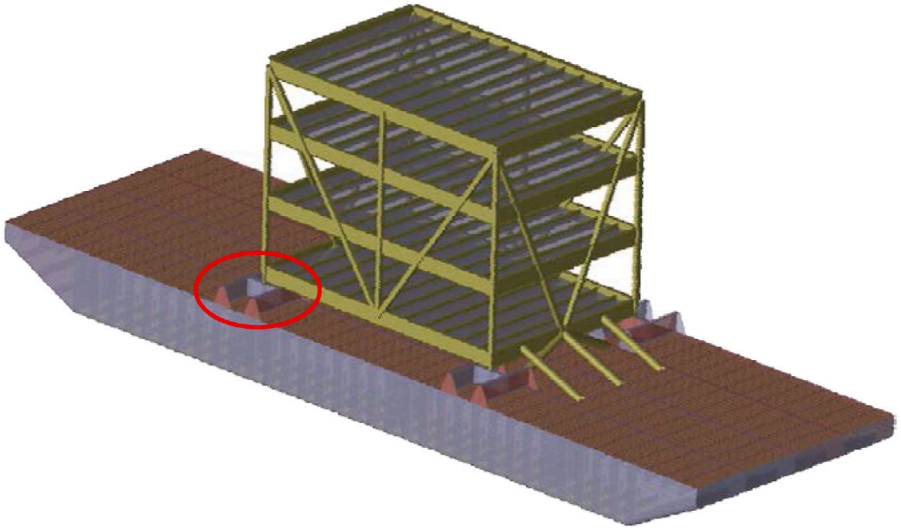

Fig. 1. Typical flat-top barge with grillage and seafastening (roll and pitch stoppers) and the transported object (only structural steel is shown, not the mechanical equipment or outfitting structures).

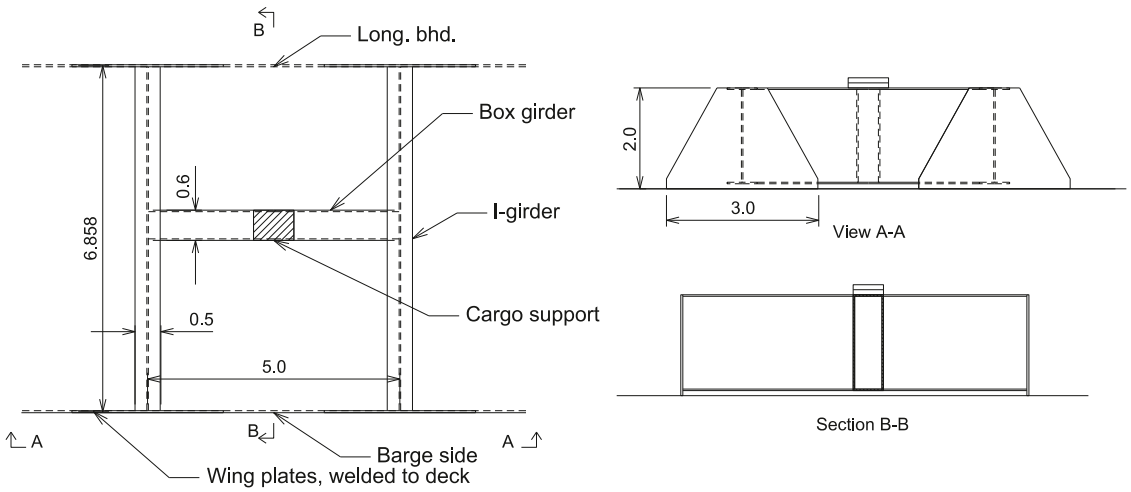

Fig. 2. Plan view of the grillage beams, a box girder and two I-girders in the vertical support (see the red ring in Fig. 1). The grillage beams are connected to the barge deck by brackets located in-line with longitudinal bulkheads and the barge side. Typical dimensions for the barge transport of a heavy object of 3500 tonnes are given (unit, meters). Typical grillage beams would be made by welded steel plates with a yield stress of 355 MPa, a flange thickness of 40–50 mm and a web thickness of 30–40 mm, with local reinforcements as required (the connection toward the deck varies depending on the ship's local strength).

seas, corresponding to $\theta = 90°$. In the case of a tug breakdown or towline failure, the barge drifts and may turn 90 degrees to the wave direction. Beam sea exposure is therefore taken to be the governing wave direction.

2.4.2. Failure modes

The following ultimate limit state failure modes are considered:

- structural failure of the barge;
- structural failure of the transported object; and
- structural failure of the vertical supports.

The capacity limits of the critical structural components are discussed in Section 2.8. Fatigue failure, collapse due to accidental loads (caused by, e.g., human error), the effect of local damage/corrosion, and accidental heel/trim due to water ingress are not considered.

2.5. Design of structural components

2.5.1. Calculation of characteristic forces

The governing load effects due to static loads and wave-induced barge motions must be calculated as inputs to the structural design. The support forces can be found from a hydrodynamic analysis using a 3D panel model, where the characteristic load is calculated as, e.g., the most probable maximum value or expected maximum value during a suitably selected sea state. That analysis is not performed here. To investigate the implicit safety level by use of a practical design approach, the method in the standard for marine operation DNVGL-ST-N001 (2020) is used to calculate the characteristic dynamic loads in the vertical support.

Wind contributes to the design load and could be included in the reliability analysis. Because the wind load is relatively small, however, the impact on the reliability is also relatively small; thus, the wind is not included in the analyses.

2.5.2. Design criteria in ultimate capacity analysis

The structural design is based on a standard capacity equation in the ultimate limit state. Here, we consider the static load effect from gravity and the dynamic load effect from the wave-induced motions of the barge. The capacity check is expressed as follows:

$$\frac{R_c}{\gamma_m} \geq \gamma_G S_{c,G} + \gamma_E S_{c,E} \tag{1}$$

Table 1
Load coefficients in the ultimate limit state according to, e.g., DNVGL-ST-N001 (2020). *G = permanent actions (e.g., due to self-weight) and E = environmental actions (e.g., due to wave-induced loads).

Action combination	Load coefficients	
	γ_G	γ_E
ULS-A	1.3	0.7
ULS-B	1.0	1.3

R_c is the characteristic capacity, generally defined as the 5% fractile value, see, e.g., EN 1990 (2005) or DNVGL-ST-N001 (2020). γ_m is the material factor, equal to 1.15 for steel structures according to DNVGL-ST-N001 (2020). $S_{c,G}$ and $S_{c,E}$ are the characteristic static and dynamic load effects, respectively. The characteristic load effects used in the case studies are given in Section 3.1.2. The load factors for the ultimate limit state are given in Table 1. The load and material factors correspond to a specific reliability index that is not known and is investigated as part of this work.

The sea transports considered here are custom-made, nonroutine transports. The design of the seafastening system is assumed to fulfill Eq. (1); hence, we have

$$R_c = \gamma_m(\gamma_G S_{c,G} + \gamma_E S_{c,E}) \tag{2}$$

where the parameters are defined in relation to Eq. (1).

2.5.3. Structural elements in the seafastening system

The structural elements specially designed for marine transports are typically grillage beams to transfer the vertical load into the transport vessel and braces to transfer the horizontal loads from the rolling and pitching of the vessel. We consider the vertical load transfer, and typical structural components are

- grillage beams constructed by I-girders or box girders;
- the connection between the grillage beams and the barge deck, typically made of wing plates welded to the vessel deck to distribute the load into web frames and bulkheads; and
- stiffened plate panels in the bulkheads.

2.6. Structural reliability analysis

2.6.1. Reliability formulation

The reliability analysis methods are described in detail by, e.g., Madsen et al. (1986) and Melchers and Beck (2018). A brief account is given below. The limit state function, or failure function, $g(\boldsymbol{X})$, is defined for a particular problem, where $g(\boldsymbol{X}) \leq 0$ represents failure. The probability of structural failure is expressed as follows:

$$\begin{aligned} P_f &= P(g(\boldsymbol{X}) \leq 0) = \int \dots \int_{g(\boldsymbol{X})\leq 0} f_{\boldsymbol{X}}(\boldsymbol{x})\,\mathrm{d}\boldsymbol{x} \\ &= \int \dots \int_{\boldsymbol{X}} I[g(\boldsymbol{x}) \leq 0] f_{\boldsymbol{X}}(\boldsymbol{x})\,\mathrm{d}\boldsymbol{x} \end{aligned} \tag{3}$$

where $I[\ ]$ is an indicator function equal to 1 if [ ] is "true" and 0 if [ ] is "false". $\boldsymbol{X}$ is a vector of variables representing the load effects and the capacity. $f_{\boldsymbol{X}}(\boldsymbol{x})$ is the joint probability density of all the variables involved.

Equivalent to the failure probability, we can report the reliability index, $\beta = -\Phi^{-1}(P_f)$, as a safety measure, where $\Phi()$ is the cumulative distribution function for the standard normal distribution.

The integral in Eq. (3) can be solved by numerical integration by the first- or second-order reliability method (FORM/SORM) or by Monte Carlo simulation. The SORM is used to calculate the failure probabilities in the case studies in Section 3, and the results are spot checked by Monte Carlo simulations. The calculations are performed using the computer program Proban (Tvedt, 2006).

When modeling the structural capacity and the load effect by stochastic variables, R and S, respectively, the failure function can be expressed simply as follows:

$$g(\boldsymbol{X}) = R - S \tag{4}$$

While the capacity check in Eq. (2) is semiprobabilistic, Eq. (4) represents the capacity check in a probabilistic format. When R and S are statistically independent, we have $f_{\boldsymbol{X}}(\boldsymbol{x})\mathrm{d}\boldsymbol{x} = f_{\boldsymbol{R}}(\boldsymbol{r})f_S(\boldsymbol{s})\mathrm{d}\boldsymbol{r}\mathrm{d}\boldsymbol{s}$ in Eq. (3).

The structural capacity can be expressed by a random variable, R, as follows:

$$R = \chi_R R_c \tag{5}$$

where

- χ_R is a variable to account for uncertainties in the ultimate capacity model, see Section 2.8, and
- R_c is calculated from Eq. (2).

The load effect is expressed by a random variable, S, as follows:

$$S = \chi_{S,G} S_G + \chi_{S,E} S_E \tag{6}$$

where

- S_G is the static load effect, taken equal to $S_{c,G}$ in Eq. (2);
- $\chi_{S,G}$ is a random variable representing the uncertainty in the calculated static load effect, see Section 2.7.2;
- $\chi_{S,E}$ is a random variable representing the uncertainty in the calculated wave-induced vessel motions and the corresponding load effects in the seafastening system; see Section 2.7.3;
- S_E is the wave-induced load effect; see Section 2.7.4 (note that this term is not the same as $S_{c,E}$ in Eq. (2) in Section 2.5.1);

2.6.2. Uncertainty importance factors

The uncertainty importance factors provide information on the influence of the variables in $g(\boldsymbol{X})$ from Eq. (4) on the failure probability. The importance factors represent the percentage of the total uncertainty in the reliability index, β, due to the corresponding random variable or group of random variables. The importance factors are defined as $100\alpha_i^2$, where α_i are the sensitivity factors, which are defined as follows, see, e.g., Madsen (1988):

$$\alpha_i = \frac{\partial \beta}{\partial u_i}\Big|_{\boldsymbol{u}^*} \tag{7}$$

The importance factors are calculated by FORM, where the variables are transferred to u-space, u_i are random variables with a standard normal distribution, and $\boldsymbol{u}^*$ is the design point in u-space. If an importance factor is low, the uncertainty in the corresponding variable has little effect on the failure probability.

2.7. Load effect modeling

2.7.1. Variables included in the analysis

The statistical uncertainties in the variables included in the reliability analysis are discussed below. The following variables are included:

- the static load effect uncertainty, $\chi_{S,G}$ (Section 2.7.2);
- the dynamic load effect uncertainty, $\chi_{S,E}$ (Section 2.7.3);
- the wave-induced load effect, S_E (Section 2.7.4);
- the significant wave height, H_s (Section 2.7.5); and
- the wave period, T_z (Section 2.7.6);

The uncertainty variables are modeled by normal distributions ($\chi_{S,G}$ and $\chi_{S,E}$) with the estimated bias and coefficient of variation (COV). The bias is the mean value of the random variable, μ_χ, and is defined as the ratio between the true and estimated values of the variable. The COV is defined as σ_χ/μ_χ, where σ_χ is the standard deviation of the variable.

2.7.2. Uncertainty in the calculated static load effect, $\chi_{S,G}$

The characteristic load effect from gravity, $S_{c,G}$, is calculated based on the maximum expected weight of the transported object. The load distribution between the supports depends on the elasticity of the supports, fabrication tolerances, etc. The load distribution can also depend on the ballast condition of the barge after the transported object is set down. Such effects are not included here, and the weight is simply divided between four supports. The transported object is usually weighed upon completion; hence, prior to transport, the actual weight is known with high accuracy. Assuming a conservative approach in the design phase—i.e., the estimated values are on the high side—a bias in the weight is expected. In the case studies, $\chi_{S,G}$ is modeled as a normally distributed variable with a mean value of 0.95. The COV is set equal to 0.1.

2.7.3. Uncertainty in the calculated dynamic wave-induced load effects, $\chi_{S,E}$

The uncertainty in the calculated dynamic wave-induced load effects, $\chi_{S,E}$, depends on

- the wave data (as discussed above);
- the calculated motions of the transport vessel, $\chi_{S,E,1}$; and
- the method for calculating the structural load effects due to vessel motions, $\chi_{S,E,2}$.

The last two items are included here, and the resulting uncertainty is estimated by $\chi_{S,E} = \chi_{S,E,1} \cdot \chi_{S,E,2}$. In Natskår and Steen (2013), the support forces calculated from motion analyses and from model tests were compared, and a bias was estimated by comparing the standard deviations and maximum values of the response. The bias was estimated at 0.75–0.94 (bias <1, i.e., conservative analysis results) for the maximum roll angle and 0.65–0.8 for the vertical support force, depending on the type of analysis. These model tests were performed in severe seas; some of the sea states had very steep waves, and there were nonlinear effects that limited the barge response in the model tests (water on deck, etc.). In the current study, we need a bias representative of all sea states included in the long-term distribution. Hence, for $\chi_{S,E,1}$, a moderate bias of 0.9 is chosen for the given environmental conditions using a linear analysis with a stochastic linearization of viscous roll damping. The uncertainty is assumed to follow a normal distribution with a COV of 0.1. The uncertainties in the calculated load effects, $\chi_{S,E,2}$, are assumed to be the same as for the static load effect—i.e., a mean value of 0.95 and COV of 0.1 (see above). Note that even if a simple statistical uncertainty model suffices for beam seas, in a real case, the uncertainty could depend on the ballast condition, the relative stiffness between the supports, and the wave direction. The resulting uncertainty, $\chi_{S,E}$, has a mean value of 0.86 and a COV of 0.14. (For the product of two statistically independent variables, $\chi = \chi_1 \cdot \chi_2$, the mean value is $\mu_\chi = \mu_{\chi 1} \cdot \mu_{\chi 2}$ and the coefficient of variation is $\mathrm{COV} \approx \sqrt{(\mathrm{COV}_{\chi_1})^2 + (\mathrm{COV}_{\chi_2})^2}$; see, e.g., Melchers and Beck (2018).)

2.7.4. Wave-induced load effects, S_E

The wave-induced load effect is derived from vessel motion calculated by potential theory for a 3-D panel model of the barge using the computer program package (SESAM, 2019). In principle, the barge is subjected to wind seas and swells. However, the period of swell is (much) larger than the roll period, which is of main importance, and the dynamic effects will be limited. Moreover, the accelerations in long-periodic motions are relatively small. Hence, the current study considers wind sea only. The analysis is based on linear theory, and nonlinear roll damping due to eddy making is not included in the hydrodynamic analysis. This damping is included by stochastic linearization of the quadratic viscous damping. The wave-induced seafastening loads are calculated by requiring dynamic equilibrium of the transported object exposed to the barge motions/accelerations calculated in the hydrodynamic analysis; see Natskår and Steen (2013). Because the calculation of forces is based on a simple equilibrium of the cargo, uncertainties arise due to the interaction between the cargo and the barge. However, if the center of gravity is close to or at the geometric center and we consider beam seas, such a simplified approach can produce good results. In principle, this calculation also involves uncertainties in S_G and S_E (as mentioned in Sec. Section 2.7.3).

The statistical distribution of the individual response maxima is defined as follows; see, e.g., Naess and Moan (2013):

$$F_{S_E}(s_E) = \int_0^\infty \int_0^\infty F_{S_E|H_s,T_z}(s_E|h_s,t_z) f_{H_s,T_z}(h_s,t_z)\,\mathrm{d}h_s\,\mathrm{d}t_z \tag{8}$$

where

- $F_{S_E|H_s,T_z}(s_E|h_s,t_z)$ is the cumulative distribution of the extreme value for the individual support force conditional on the significant wave height and the mean zero-crossing wave period and
- $f_{H_s,T_z}(h_s,t_z)$ is the joint probability density function for the significant wave height and the mean zero-crossing wave period.

The distribution of the individual response maxima within a sea state—i.e., for a given H_s and T_z—is assumed to be the extreme value distribution according to the Rayleigh distribution:

$$F_{S_E|H_s,T_z}(s_E|h_s,t_z) = \left(1 - \exp\left[-\frac{1}{2}\left(\frac{s_E}{\sigma_{S_E}(h_s,t_z)}\right)^2\right]\right)^{N(h_s,t_z)} \tag{9}$$

$\sigma_{S_E}(h_s,t_z)$ is the standard deviation, or the RMS value, of the support force. Numerical values are given in the case studies in Section 3.1.5. The total number of response cycles during marine operation for a given sea state is $N(h_s,t_z) = T_R \cdot \nu_0^+(h_s,t_z)$, where T_R is the duration of the operation and $\nu_0^+(h_s,t_z)$ is the mean zero-upcrossing rate of the response. The mean zero-upcrossing rate of the vertical support force in beam sea conditions is practically independent of the significant wave height for the barge transport we consider in the case studies below. Hence, $N(t_z) \approx T_R \nu_0^+(t_z)$, where $\nu_0^+(t_z)$ can be estimated by fitting, e.g., an exponential curve to the actual upcrossing rate; see Section 3.1.6. In reality, the duration of a marine operation is a stochastic variable; however, here it is treated as a deterministic value.

The joint probability density function of H_s and T_z is expressed by the relation

$$f_{H_s,T_z}(h_s,t_z) = f_{T_z|H_s}(t_z|h_s) f_{H_s}(h_s) \tag{10}$$

2.7.5. The significant wave height

The statistical description of the significant wave height depends on the category—i.e., if the operation is weather-restricted or weather-unrestricted. Operations with a planned duration of not more than 72 h (not more than 96 h when contingency time is included) can be defined as weather-restricted. The significant wave height to be used in the design of the operation, $H_{s,design}$ (also called the operational limit, $H_{s,op.lim.}$), is defined (chosen) during the planning of the operation. The operation can commence when the forecasted significant wave height is lower than the operational limit with a defined safety margin. This is the Alpha factor method, where $H_{s,forecast} \le \alpha \cdot H_{s,design}$, and $\alpha \le 1$. α is given in DNVGL-ST-N001 (2020)). Operations with planned durations longer than 72 h must be defined as weather-unrestricted, and the design significant wave height to be used in the planning of the operation is based on long-term wave data statistics. (Weather forecasts are still received regularly, typically every 12 h, but the operation cannot be aborted; one example is that of overseas transport.) For both categories, the inherent uncertainties in the significant wave height are accounted for. For weather-restricted operations, there are uncertainties in

- the forecasted H_s and
- the forecasted wave period, T_z. The forecasted wave period is not used in this study; instead, the statistical distribution of T_z conditional on H_s is used; see Section 2.7.6.

For weather-unrestricted operations, we have

- data uncertainty in H_s and
- fundamental variability in the long-term distribution.

Long-term data for sea states are subject to statistical uncertainty when the dataset is limited to only a few years (Moan et al., 2005). The present study is based on 60 years of hindcast data (Section 3.1.8), and the statistical uncertainty is therefore neglected.

For weather-restricted operations, the significant wave height is based on weather forecasts. The actual (true) significant wave height during a marine operation is described by a lognormal distribution (see, e.g., Bury (1999)) as follows:

$$f_{H_s}(h_s) = \frac{1}{h_s \cdot \sigma_{\ln H_s}\sqrt{2\pi}} \exp\left[-\frac{1}{2}\left(\frac{\ln h_s - \mu_{\ln H_s}}{\sigma_{\ln H_s}}\right)^2\right] \tag{11}$$

The parameters in the distribution are (see, e.g., Natskår et al. (2015))

$$\mu_{\ln H_s} = \ln(h_{s,fc}) + \mu_{\ln \chi} \tag{12a}$$

$$\sigma_{\ln H_s} = \sigma_{\ln \chi} \tag{12b}$$

where $h_{s,fc}$ is the maximum forecasted significant wave height during the operation, given in meters. The stochastic variable χ represents the uncertainty in the weather forecasts ($\chi = H_{s,hindcast}/H_{s,forecast}$). Numerical values are given in Table 6.

Long-term statistics are used for weather-unrestricted operations because the significant wave height cannot be based on weather forecasts. The significant wave height is assumed to follow a three-parameter Weibull distribution (see, e.g., Bury (1999)) as follows:

$$f_{H_s}(h) = \begin{cases} 0 & \text{if } h \le c, \\ \frac{b}{a}\left(\frac{h-c}{a}\right)^{b-1} \exp\left[-\left(\frac{h-c}{a}\right)^b\right] & \text{if } h > c. \end{cases} \tag{13}$$

From this distribution, it follows that $P(H_s \le c) = 0$; i.e., H_s is never lower than c. The parameters, a, b and c, are calculated based on hindcast data; see Section 3.1.8. The value of the parameter c is on the order of 0.5–1.0 m, and the probability density function represents the wave heights that play a role in the calculation of the P_f well.

Hindcast data are used in this study to quantify the uncertainty in weather forecasts and to calculate the long-term distribution of the significant wave height. As mentioned above, the statistical uncertainty of the long-term sea state data is neglected. The uncertainty in the forecasted significant wave height is estimated by comparing one year of forecast and hindcast data. The limited duration and uncertainty in the hindcast data may therefore affect the results. The accuracy of the hindcast significant wave height compared to measurements was studied by Haver (1994). The difference between the hindcast and measured H_s had a standard deviation of 1.15 m, based on 168 storm events with $H_{s,hindcast} \ge 7.5$ m. No clear dependence on the wave height was observed. However, we are mainly interested in lower wave heights, typically with H_s values of 3–5 m, and assuming that the accuracy has improved over the years, the uncertainty is expected to be lower in our case. According to Brooker et al. (2004), a scatter index (i.e., the standard deviation of the difference between measured and modeled H_s values normalized by the mean of the observations) of 10%–15% for significant wave heights from hindcast data is representative of modern hindcasts compared with measured values. A comparison study of hindcast data with measurements was performed by Bruserud and Haver (2016). They found the hindcast significant wave height from NORA10, as described by Reistad et al. (2011), to be slightly conservative compared with measurements. However, the difference was small, and they did not correct the hindcast significant wave height. The same trend was observed by Haakenstad et al. (2020) when comparing NORA10 data with measurements for the North Sea, the Norwegian Sea and the Barents Sea. The conclusion for our study is that even if the hindcast values are not exact, the deviation from the measured H_s-values is moderate, and the uncertainty in hindcast H_s is not included in the current study.

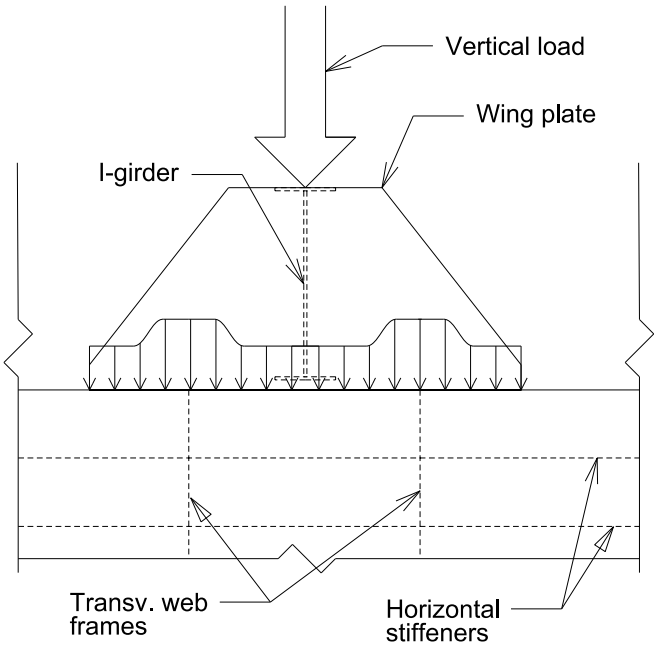

Fig. 3. Transfer of vertical force from the I-girder via the wing plates and to the vessel bulkhead. The load is transferred as a nonuniformly distributed load (indicated by arrows), with the full yield stress at the transverse web frames and a buckling stress in the center part of the plate. The distance between the transverse web frame is b, and the distance between the horizontal stiffeners is s.

2.7.6. Wave period

The wave period is described in the reliability analyses by a lognormal distribution, as shown by, e.g., Bitner-Gregersen and Haver (1991). The distribution of the mean zero-crossing period, T_z, follows a lognormal distribution that is conditional on H_s:

$$f_{T_z|H_s}(t_z|h_s) = \frac{1}{t_z \cdot \sigma_{\ln T_z|H_s}\sqrt{2\pi}} \exp\left[-\frac{1}{2}\left(\frac{\ln t_z - \mu_{\ln T_z|H_s}}{\sigma_{\ln T_z|H_s}}\right)^2\right] \tag{14}$$

The mean value and the standard deviation for $\ln(T_z)$ are calculated as follows:

$$\mu_{\ln T_z|H_s} = a_1 + a_2 h_s^{a_3} \tag{15a}$$

$$\sigma_{\ln T_z|H_s} = b_1 + b_2 e^{b_3 h_s} \tag{15b}$$

The parameters a_i and b_i, $i = 1, 2, 3$, are estimated from hindcast data and are given in Section 3.1.9.

2.8. Resistance modeling, χ_R

2.8.1. Design of the grillage and seafastening

A typical grillage beam structure for the transport of heavy objects is shown in Fig. 2. The support point for the transported object is located on the box girder, which has internal reinforcement at the support point for the transported object. The box girder transfers the load to two I-girders. At each of the ends of the I-girders, there is an end plate welded to the deck of the transport vessel, in line with the longitudinal bulkheads or the barge side; see Fig. 2. We consider the structural capacity of the grillage beams and the attachment points (bulkheads) in the transport vessel. The uncertainty in the capacity is divided into

- uncertainty in the material parameters and
- model uncertainty.

2.8.2. Uncertainty in the calculated capacity of the grillage beams

The grillage beams are exposed to shear force and bending moment, which, for the example shown in Fig. 2, can be found by hand calculations. For more complicated structures, a linear finite element analysis

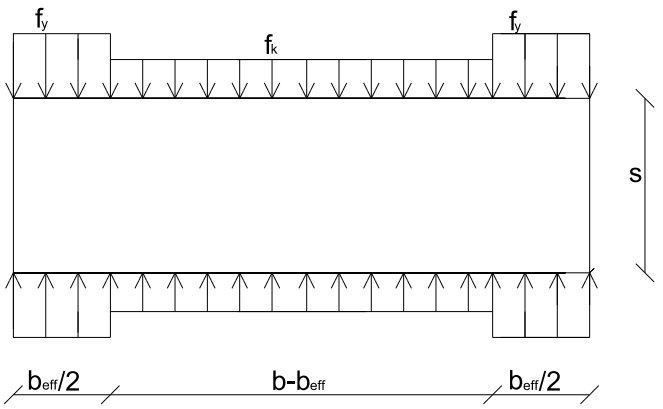

Fig. 4. One plate field with a thickness t and dimensions $b \times s$ with the model of the vertical stresses indicated.

would typically be run. The model uncertainty in the shear and bending capacity typically has a mean value of 1.0 and a COV of 0.05 (see JCSS (2000), Table 3.9.1).

The uncertainty in the material parameters—i.e., the yield stress—can generally be modeled with a mean value range of 1.05 to 1.15 and a COV range of 0.05 to 0.1; see, e.g., Moan (1995). We calculate the bias and COV according to JCSS (2000). For steel with a characteristic yield stress (the 5% fractile) equal to 355 MPa (typical steel quality for seafastening steel), the mean value is 378 MPa, i.e., a bias of 1.07. The COV is 0.07.

The resulting uncertainty, including both the model and material uncertainty, has a mean value of 1.07 and a COV of 0.09. This model, with a lognormal distribution, represents χ_R for the grillage beams.

2.8.3. Uncertainty in the calculated capacity of the bulkhead

Bulkheads with stiffeners and web frames are shown in Fig. 3. The capacity of the stiffened plate panels can be calculated according to, e.g., DNV-RP-C201 (2010). For in-plane loading parallel to the stiffeners and lateral loading on the plate plane, the model uncertainty in the calculated capacity can be described by a lognormal distribution with a mean value of 1.21 and a COV of 0.15 (see SSC-433 (2004), Table 5.1). We are not aware of such information for a load acting perpendicular to the stiffeners. We discuss two failure modes for stiffened plate panels:

- local buckling of plates between stiffeners and
- failure of stiffeners.

Uncertainties related to any reduced capacity due to corrosion or local damage are not included here.

The bulkhead is loaded from the wing plate welded to the deck (see Fig. 3). The capacity of the plate (e.g., in kN/m) is not uniform over the plate width b. Toward the edge, buckling does not occur, and the plate can be loaded until yield; see Fig. 4. In the central part of the plate, the capacity is limited by the buckling of the plate. The capacity of the bulkhead can be formulated as follows:

$$N = f_y t b_{eff} + f_k t (b - b_{eff}) \tag{16}$$

This capacity formula is similar to Eq. 6.6 in DNV-RP-C201 (2010). t is the plate thickness. The first term represents the full yield capacity at the plate edges over a length $b_{eff}/2$ at each end, and the second term represents the buckling capacity over the central part of the plate, with length $b - b_{eff}$. The buckling stress capacity, f_k, is calculated by idealizing the central part of the plate as a column with length s, where s is the center distance between the horizontal stiffeners. The buckling capacity of the central part of the plate is (for reduced slenderness, $\bar{\lambda}_c < 2.0$; see Eq. 6.7 in DNV-RP-C201 (2010)) calculated similar to buckling curve "A" in, e.g., EN 1993-1-1 (2005). In this calculation,

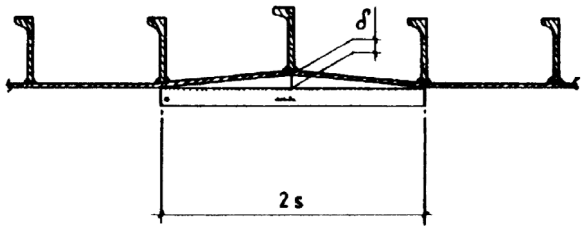

Fig. 5. Fabrication tolerance between stiffeners from DNVGL-OS-C401 (2019). The maximum misalignment allowed is $\delta = 0.02s$, where s is the center distance between the stiffeners.

the plate edges are assumed to be simply supported, i.e., they are free to rotate. In reality, there is some restrained rotation of the plate edge, and the assumption that the edges are free to rotate is conservative; hence, in reliability analyses, the bias is larger than one.

The purpose of the stiffeners is to provide support for bulkhead plates of size $b \times s$, i.e., to prevent global buckling of the bulkhead plates. Imperfections from fabrication result in a lateral load on the stiffeners. The loading mechanism is shown in Fig. 5, where the fabrication tolerance for the misalignment of one stiffener relative to the adjacent stiffeners is given. The lateral load (i.e., out-of-plane load) on the stiffeners can be calculated from Eq. 7.8 in DNV-RP-C201 (2010). The lateral load is resisted by a shear force and bending moment in the stiffeners, which indicates that standard measures for the uncertainty in the capacity model could be applied. However, the load is not the vertical load applied directly on the bulkhead but a lateral load calculated as a function of the vertical load, the geometry of the stiffeners, etc. Assuming that the uncertainty in the lateral load is accounted for through the variables $\chi_{S,G}$ and $\chi_{S,E}$, the resulting bias and COV of the calculated stiffener capacity are assumed to follow the uncertainty for ordinary beams in bending; see Section 2.8.2.

To summarize, the bulkhead capacity for a vertical load is limited by

- yielding at the edges of the bulkhead plate,
- buckling in the mid part of the bulkhead plate, and
- buckling of the stiffeners due to second-order deformation.

We conclude that the capacity model for the bulkheads should not be different from the case with axial loading parallel to the stiffeners or the case of lateral loading. The model uncertainty is therefore taken from SSC-433 (2004) as lognormally distributed with a mean value of 1.21 and a COV of 0.15.

Similar to the steps performed in Section 2.8.2, the mean value of the yield stress is calculated according to JCSS (2000). For steel with a characteristic yield stress equal to 235 MPa (typical steel quality for barges), the bias is found to be 1.04, and the COV is 0.07. The uncertainty in the calculated capacity of the bulkhead is modeled with a mean value of 1.25 and a COV of 0.17.

2.8.4. Capacity of the transported object

The capacity of the transported object should be checked. Sea transport is typically included in the engineering phase, where it is checked together with the in-place condition. However, those analyses are not included here.

2.8.5. Resulting uncertainty in the structural capacity

Based on the previous discussion, the uncertainty of the grillage beams is modeled with a bias of 1.07 and a COV of 0.09. The bulkhead uncertainty is described by a bias of 1.25 and a COV of 0.17. Despite the higher bias, the bulkhead is associated with a larger failure probability because of the larger COV. Hence, the values for the bulkhead are used in the case studies; see Table 4. A sensitivity study with variable bias and COV is included in Section 3.6.

2.9. Target reliability level during temporary phases

Decision making relating to the reliability of structures involves an assessment of the reliability as outlined above as well as evaluating the reliability in view of a target reliability level. This section deals with the basis for establishing a target reliability level. In transport operations using towed barges, the barges are usually unmanned, and only material damage is considered. A severe structural failure resulting in the total loss of the handled object will lead to economic losses due to the cost of replacing the lost asset. It could also be expensive to recover the lost object and scrap it. In addition, there could be indirect costs due to delays in the production start, increased insurance costs for future projects, and a loss of future contracts for the companies involved. To define a target reliability level, the reference period must be given. For permanent offshore structures, the service lifetime may range from 20 to 100 years, while a marine operation typically will have a duration of a few hours up to a few weeks. For a permanent structure, it is convenient to relate the target reliability levels to an annual failure probability. With a similar approach for marine operation, the failure probability per operation depends on the duration. From an insurance point of view, it is more convenient to define the failure probability per operation, independent of the duration. For fatalities, the target probabilities could be given per year, but that aspect is not considered here. For a structure under operating conditions, the recommended target levels for annual failure probabilities, depending on the consequence of failure, are given, e.g., in ISO 2394 (2015). The target levels for failure probability in temporary conditions can also reflect the consequences of failure. The target level could, for example, be defined per operation based on the following aspects:

- risk of fatalities, e.g., whether a towed barge is manned or unmanned;
- risk of environmental pollution;
- risk of economic loss (e.g., target level depending on the value of the transported object); and
- consequential losses, e.g., delayed start of production.

Such an approach is not used by DNVGL-ST-N001 (2020) for marine operations. Instead, a constant target level for the failure probability is given. The probability of structural failure leading to a total loss should be less than 10^{-4} per operation. This level was first given in the *Standard for Insurance Warranty Surveys in Marine Operations* issued by DNV in 1985. Even if this threshold was not very rigorously determined, it has since been accepted by the industry and insurance companies. The calculated failure probabilities are sensitive to the assumptions they are based on—e.g., the bias and COV of the variables involved—so the calculated failure probability can deviate from the recommended target levels. However, in the case studies in Section 3, the absolute probability is not of main interest; it is the relative failure probability—e.g., for various durations of an operation—that is of greatest interest.

3. Case studies

3.1. System modeling

3.1.1. General

We consider a transport barge loaded with a large object, as shown in Fig. 1. The barge is a flat-top barge with dimensions of 91.4×27.4×6.1 m and a raked bow and stern. The draft is 3 m, and the natural period in rolling is 8.5 s. Viscous roll damping is included through equivalent stochastic linearization. The transported object has a length of 30 m, a width of 20 m and a height of 20 m, with a uniformly distributed mass and the center of gravity at the geometric center. The mass is 3500 tonnes. The object is placed on 2-m high grillage beams on the barge. More information about this case is given by Natskår and Steen (2013).

Table 2
Characteristic load effects in the vertical support due to wave-induced barge motion according to DNVGL-ST-N001 (2020). The forces are scaled by mg, where m is the mass of the transported object and $g = 9.81$ m/s^2.

Condition	$S_{c,E}$
1. Unrestricted	0.268 mg
2. $H_s = 6$ m	0.235 mg
3. $H_s = 4$ m	0.195 mg

Table 3
Maximum allowed forecasted H_s according to DNVGL-ST-N001 (2020), based on the design significant wave height, $H_{s,d}$, equal to 4 and 6 m.

No. of days	T_R (h)	Max. $H_{s,Oper}$ (m)	
		$H_{s,d} = 4$ m	6 m
1	24	3.0	4.7
2	48	2.8	4.4
3	72	2.7	4.3

The following case studies are included in Section 3.2–3.6:

1. For weather-restricted transport, the failure probability is calculated as a function of the duration and the forecasted wave height. The failure probabilities are calculated with and without accounting for the uncertainty in the weather forecasts (Case 1).
2. For weather-unrestricted transport, the failure probabilities are compared for operations executed in July and October (Case 2). Furthermore, we calculate the failure probability for the execution of the transport in each of the months within the autumn season (Case 3). We then compare the use of seasonal and year-round data (Case 4).
3. The sensitivity is studied through the failure probability and the importance factors for a base case and for variations in the random variables.

3.1.2. Characteristic load effects in the supports

The characteristic load effects in the ultimate limit state are calculated for the following three conditions:

1. Weather-unrestricted transport worldwide;
2. Significant wave height limited to 6 m; and
3. Significant wave height limited to 4 m.

In a previous version of the DNV standard for marine operations (DNV-OS-H202), it was indicated that the standard acceleration for $H_s = 6$ m (Condition 2 in Table 2) could be used for weather-unrestricted transport during the summer (June–August) in the North Sea. This fits well with the one-year return period significant wave heights, as given in Table 7 below. See also Section 3.3.

For the transported object with mass m and geometry as given in Section 3.1.1, the vertical characteristic support reactions, $S_{c,E}$, due to roll motion are presented in Table 2 for weather-unrestricted transport and for transports with significant wave heights limited to 6 and 4 m. The vertical static load effect at each support is $S_{c,G} = 0.25mg$ (because we have assumed that the center of gravity is located at the geometric center of the transported object). Based on these characteristic forces, the required structural capacity—i.e., R_c in Eq. (2)—is calculated.

It is emphasized that the environmental load effects in Table 2 are not based on a stochastic analysis. They are not described by a probability distribution, and they do not depend on the duration of the operation. They are deterministically calculated characteristic loads from a design standard to be applied directly in Eq. (2).

3.1.3. Forecast uncertainty

The characteristic load effects for H_s equal to 4 and 6 m are given in Table 2. Because of the forecast uncertainty, the forecasted significant

Table 4
Mean value and COV of the variables in the case studies.

Variable	Description	Distribution	Mean	COV
χ_R	Uncert. in the structural capacity of the bulkhead	Lognormal	1.25	0.17
R_c	Characteristic structural capacity	Fixed	Eq. (2)	–
$\chi_{S,G}$	Uncert. in the calculated static load effect	Normal	0.95	0.1
$\chi_{S,E}$	Uncert. in the calculated dynamic load effect	Normal	0.86	0.14
S_E	Vertical dynamic load effect	See Eq. (8)	–	–
H_s	Significant wave height	See Section 2.7.5	–	–
T_z	Mean zero-crossing wave period	See Section 2.7.6	–	–
ν_0^+	Mean zero-upcrossing rate of the response	See Eq. (20)	–	–

Table 5
Numerical values for the parameters k_{ij} in Eq. (19).

i	k_{i1}	k_{i2}	k_{i3}
1	$2.56 \cdot 10^{-3}$	$2.44 \cdot 10^{-4}$	$-1.91 \cdot 10^{-5}$
2	$2.59 \cdot 10^{-2}$	$-2.57 \cdot 10^{-3}$	$7.21 \cdot 10^{-5}$
3	$-7.73 \cdot 10^{-4}$	$9.47 \cdot 10^{-5}$	$-3.01 \cdot 10^{-6}$

wave height prior to the start of an operation must be lower than the design H_s—i.e., the value of H_s used to calculate the vessel motion and support forces. The maximum allowed forecasted significant wave heights are given in Table 3.

3.1.4. Failure function for the reliability analysis

The failure function for calculating the probability of failure from Eq. (3) is as follows:

$$g() = \chi_R R_c - (\chi_{S,G} S_G + \chi_{S,E} S_E) \tag{17}$$

where the parameters are defined in relation to Eqs. (5) and (6). Information for the variables is given in Table 4.

3.1.5. Load effects to be used in the reliability analysis

The wave-induced load effect in a vertical support is described by the standard deviation of the response as a function of the significant wave height and the mean zero-crossing wave period, $\sigma_{S_E}(h_s, t_z)$. The standard deviation is represented by a response surface given as follows (see, e.g., Rajashekhar and Ellingwood (1993)):

$$\sigma_{S_E}(h_s, t_z) = (A_1(t_z) + A_2(t_z)h_s + A_3(t_z)h_s^2)mg \tag{18}$$

The standard deviation is almost linear with H_s for a given T_z, but the quadratic roll damping makes the response slightly nonlinear; hence, the H_s-squared term is included. The parameters A_1, A_2 and A_3 are calculated from:

$$A_i(t_z) = k_{i1} + k_{i2}t_z + k_{i3}t_z^2 \; for \; i = 1, 2, 3 \tag{19}$$

The coefficients, k_{ij}, for the barge in Section 3.1.1 exposed to long crested seas are given in Table 5. The response surface is an approximation, and for periods lower than 4 s, the response surface overestimates the support force. However, such low wave periods are relevant only for very small H_s-values, which do not occur often in open seas. Furthermore, even if the support force is overestimated for $T_z \leq 4$ m, it is still small and does not contribute significantly to the failure probability. The inaccuracy resulting from the fitted response surface is fairly moderate and can be represented by a variable with a mean value of 1.0 and a COV of 0.05. This inaccuracy is neglected in the case studies.

The most probable maximum support load, which is calculated based on the standard deviation of the response from Eq. (18) is shown in Fig. 6 as a function of the significant wave height. (The support load is calculated using a modified version of Eq. (8) by integrating over T_z only and solving for s from $F_{S|H_s}(s|h_s) = e^{-1}$.)

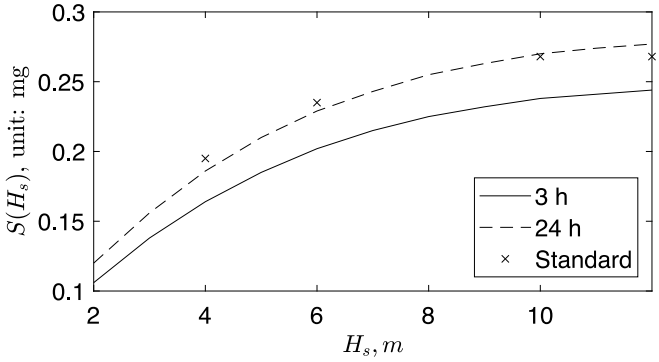

Fig. 6. Most probable maximum vertical force, $S(H_s)$, at one support point as a function of the significant wave height based on Eq. (8) for exposure times equal to 3 and 24 h. The design forces calculated according to DNVGL-ST-N001 (2020) for $H_s = 4$ m and 6 m and a weather-unrestricted transport ($H_s \geq 10$ m) from Table 2 are also shown.

Table 6
Selected numerical values for $\mu_{\ln\chi}$, $\sigma_{\ln\chi}$, μ_χ and σ_χ in the lognormal distribution for the uncertainty in the weather forecasts, based on one year with a comparison of the forecast and hindcast results in the Norwegian Sea, from Natskår et al. (2015).

No. of days	T_R (h)	$\mu_{ln\chi}$ (-)	$\sigma_{ln\chi}$ (-)	μ_χ (-)	σ_χ (-)
1	24	0.055	0.112	1.06	0.12
2	48	0.066	0.119	1.08	0.13
3	72	0.079	0.134	1.09	0.15

3.1.6. The mean zero-upcrossing rate of the response

The mean zero-upcrossing rate of the response is input into Eq. (9). The mean zero-upcrossing rate is calculated from the hydrodynamic analysis, and an exponential curve is fitted to the calculated results as follows:

$$\nu_0^+(t_z) = 0.12 + 0.87e^{-0.64t_z} \tag{20}$$

where T_z is given in seconds, and the unit for ν_0^+ is s^{-1}. This curve represents the mean zero-upcrossing rate well. The values from Eq. (20) are within ±2% of the mean zero-upcrossing rate from the hydrodynamic analysis. (For a large value of T_z, ν_0^+ converges toward 0.12 s^{-1}. This is the natural frequency of the barge in roll.)

3.1.7. Forecast uncertainty of the significant wave height

The parameters $\mu_{\ln H_s}$ and $\sigma_{\ln H_s}$ to be used in Eq. (12) are shown in Table 6 as a function of the duration of the operation.

3.1.8. Long-term distribution of the significant wave height

The long-term distribution of the significant wave height is needed for weather-unrestricted operations and is given by the Weibull distribution in Eq. (13). In this paper, we use parameters representative of the northern North Sea. The parameters are based on hindcast data (see, e.g., Reistad et al. (2011)) from a location 150 km west of Haugesund,

Table 7
Parameters in the three-parameter long-term Weibull distribution of the significant wave height (see Eq. (13)) for each month and year-round, for the northern North Sea. The significant wave height with an approximately 10% probability of being exceeded during one month is also shown.

Month	a(m)	b (-)	c(m)	$H_{s,design}$ (m)
Jan	2.87	1.58	0.88	11.6
Feb	2.67	1.57	0.70	10.7
Mar	2.39	1.52	0.75	10.2
Apr	1.60	1.30	0.72	8.6
May	1.24	1.26	0.59	7.1
Jun	1.04	1.23	0.56	6.2
Jul	0.94	1.21	0.54	5.8
Aug	1.02	1.19	0.58	6.4
Sep	1.49	1.23	0.77	8.8
Oct	2.13	1.43	0.81	10.0
Nov	2.42	1.54	0.92	10.2
Dec	2.73	1.54	0.90	11.4
All year	2.05	1.31	0.54	10.6

Table 8
Parameters in the three-parameter long-term Weibull distribution of the significant wave height (see Eq. (13)) for each season for the northern North Sea. The significant wave height with an approximately 10% probability of being exceeded during one month is also shown.

Month	a(m)	b(-)	c(m)	$H_{s,design}$ (m)
Winter (Dec–Feb)	2.77	1.56	0.82	11.3
Spring (Mar–May)	1.79	1.29	0.63	9.5
Summer (Jun–Aug)	1.00	1.20	0.56	6.2
Autumn (Sep–Nov)	2.11	1.41	0.75	10.0

Table 9
Parameters for the conditional distribution of T_z (see Eq. (15)) based on year-round data for the northern North Sea.

Parameter	a_1	a_2	a_3	b_1	b_2	b_3
Value	1.277	0.378	0.441	0.005	0.195	−0.169

Norway, from September 1957 until December 2017. The Weibull parameters are estimated by the method of moments (see, e.g., Bury (1999), Sec. 17.6). The parameters for each month and for the year are given in Table 7.

Instead of monthly data, the data may be divided into seasons, which are typically winter (December–February), spring (March–May), summer (June–August) and autumn (September–November). Seasonal data are given in Table 8.

Together with the Weibull parameters, examples of significant wave heights to be used in the design of a weather-unrestricted operation with a duration of up to one month are shown. There is an approximately 10% probability of exceeding these significant wave heights during a one-month exposure time.

3.1.9. Distribution of T_z conditional upon H_s

The conditional distribution of the mean zero-crossing wave period, T_z, is estimated from the same hindcast data as the significant wave height. While the distribution for H_s was estimated for each month and season, the year-round data are included for the distribution fitted to T_z. The values for the parameters in the lognormal distribution from Section 2.7.6 are given in Table 9.

3.2. Case 1: Seafastening designed for weather-restricted transport

3.2.1. Case description

For weather-restricted transport, we calculate the failure probability with and without considering the uncertainty in the weather forecasts according to the Alpha factor method described in Section 2.7.5. In Section 3.2.2, we assume that the supports are designed for $H_s = 6$ m according to Section 3.1.2. When the forecast uncertainty is considered according to the Alpha factor method, we perform the following:

Table 10
Case 1: The failure probabilities of the vertical supports are shown for a weather-restricted operation based on a design where $H_s = 6$ m. When the effect of the forecast uncertainty is included, P_f is calculated for a forecasted H_s equal to the maximum from Table 3 with consideration of the forecast uncertainty, as given in the column for $H_{s,fc}$. When the forecast uncertainty is excluded, $H_s \equiv 6$ m is used as a deterministic variable.

No. of days	$H_{s,fc}$ [1)] (m)	P_f	
		Uncert. excl.	Uncert. incl.
1	4.7	$1.2 \cdot 10^{-3}$	$7.3 \cdot 10^{-4}$
2	4.4	$1.6 \cdot 10^{-3}$	$7.7 \cdot 10^{-4}$
3	4.3	$1.8 \cdot 10^{-3}$	$8.9 \cdot 10^{-4}$

Note 1: With no forecast uncertainty, $H_s \equiv 6$ m.

1. The forecasted H_s to start the operation is taken according to Table 3; hence, the forecasted H_s is equal to 4.7 m for a one-day operation, 4.4 m for two days and 4.3 m for three days.
2. The uncertainty in the significant wave height is accounted for by applying the lognormal distribution according to Eq. (11), with the mean and standard deviation taken from Table 6; hence, $\mu_{ln\chi} = 0.055$ and $\sigma_{ln\chi} = 0.112$ for a one-day operation, and so on.
3. The failure probability is calculated according to Eq. (3) for 24, 48 and 72 h.

As a quick check of how reasonable the forecast limits seem, let us consider the uncertainty given in Table 6. For a forecasted significant wave height of 6 m, the mean value plus two standard deviations after 48 h is $(1.08 + 2 \cdot 0.13) \cdot 6$ m ≈ 8 m, which is well above the design H_s. When the forecast indicates a significant wave height of no more than 4.4 m over the next two days, as required above, the mean value plus two standard deviations equals 5.9 m, which is close to the design value. Hence, the reduction in the design H_s to reach the forecast H_s seems plausible.

When the forecast uncertainty is *not* considered, we do not reduce the forecast limit to start the operation; the operation starts when the forecasted H_s is equal to 6 m. This is a hypothetical situation because it implies that the weather forecasts are exact and that the true H_s is identical to the forecasted H_s. The purpose is to quantify the effect of forecast uncertainty. Under this assumption, the failure probability is calculated for one, two and three days, all with $H_s = 6$ m.

In Section 3.2.3, we perform the same steps as described above, but in this case, the seafastening system is designed for $H_s = 4$ m—i.e., according to option 3 from Section 3.1.2.

We assume that the forecasted significant wave height remains constant during the operation period. This condition does not necessarily hold, as the forecasted H_s varies over time. However, for moderate sea states, the significant wave height can be approximately the same over several consecutive days, and therefore a constant H_s during the operation is chosen.

3.2.2. Design limit $H_s = 6$ m

The maximum forecasted H_s to start the transport is 4.7 m for an operation period of one day, decreasing to 4.3 m for a period of 3 days according to the data in Table 3. The failure probability accounting for the forecast uncertainty is shown in Table 10. The failure probability without forecast uncertainty is also calculated for $H_s = 6$ m.

The failure probability increases with the increasing duration both with and without forecast uncertainty because the maximum forces (extreme values) increase over time for a given H_s. When forecast uncertainty is included, there is an additional effect because the forecast uncertainty also increases with time. However, the increased uncertainty is counteracted by the reduced forecasted H_s for longer operations. In fact, the reduced startup criterion accounts for the uncertainty and results in a lower failure probability when the forecast uncertainty is included.

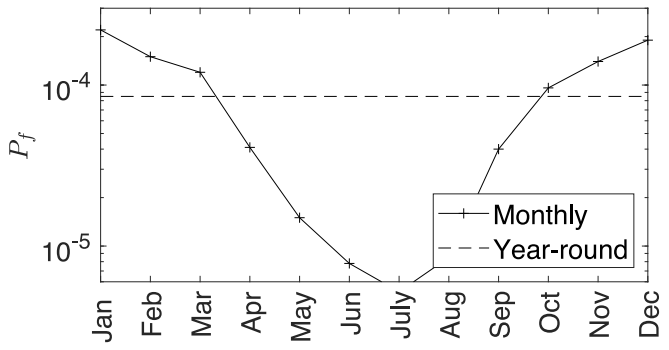

Fig. 7. Case 4: Failure probability for an operation with a duration of seven days based on monthly and year-round wave data.

Table 11
Case 1: Similar to Table 10 but with $H_s = 4$ m.

No. of days	$H_{s,fc}$[1)] (m)	P_f	
		Uncert. excl.	Uncert. incl.
1	3.0	$1.4 \cdot 10^{-3}$	$6.2 \cdot 10^{-4}$
2	2.8	$1.8 \cdot 10^{-3}$	$6.2 \cdot 10^{-4}$
3	2.7	$2.1 \cdot 10^{-3}$	$6.6 \cdot 10^{-4}$

Note 1: $H_s \equiv 4$ m with no forecast uncertainty.

Table 12
Case 2: The failure probabilities for a weather-unrestricted operation designed based on standard motion criteria, executed in July and in October.

No. of days	P_f	
	July	Oct.
3	$3.7 \cdot 10^{-6}$	$6.9 \cdot 10^{-5}$
7	$5.2 \cdot 10^{-6}$	$9.6 \cdot 10^{-5}$
14	$6.8 \cdot 10^{-6}$	$1.2 \cdot 10^{-4}$
21	$7.8 \cdot 10^{-6}$	$1.4 \cdot 10^{-4}$

3.2.3. Design limit $H_s = 4$ m

In Table 11, the failure probability accounting for forecast uncertainty is calculated for a forecasted wave height equal to the operational limit from Table 3. The failure probability without forecast uncertainty is also calculated for $H_s = 4$ m. The results compare well with the previous design case (Table 10).

3.3. Case 2: Weather-unrestricted transport executed in July and October

We now consider weather-unrestricted transport where the grillage and seafastening have been designed according to the weather-unrestricted option described in Section 3.1.2. The failure probabilities are calculated for a duration of three days to three weeks with the assumption that the operation is executed in July or October. The failure probabilities are shown in Table 12. (Note that the effect of the uncertainty in the weather forecasts is not included here. The duration is more than three days, and the operation does not depend on weather forecasts but on long-term statistical data.)

The failure probability differs substantially depending on the time of year. P_f is 18 times higher in October than in July. The failure probability increases slightly with the increasing duration and doubles as the duration increases from 3 to 21 days.

As mentioned in Section 3.1.2, DNV-OS-H202 allows the grillage and seafastening to be designed for $H_s = 6$ m for weather-unrestricted summer transport operation in the North Sea. The failure probability would then be $1.8 \cdot 10^{-5}$ for a three-day transport operation (instead of $3.7 \cdot 10^{-6}$ in Table 12), increasing to $3.4 \cdot 10^{-5}$ for 21 days. Hence, there is a better balance between transport operations in July and October (P_f is four times higher in October than in July).

Table 13
Case 3: Failure probabilities of the seafastening system for transport based on wave data for September–November and for the autumn season.

No. of days	P_f			
	Sep.	Oct.	Nov.	Autumn
3	$2.9 \cdot 10^{-5}$	$6.9 \cdot 10^{-5}$	$9.8 \cdot 10^{-5}$	$6.5 \cdot 10^{-5}$
7	$4.0 \cdot 10^{-5}$	$9.6 \cdot 10^{-5}$	$1.4 \cdot 10^{-4}$	$9.1 \cdot 10^{-5}$
14	$5.2 \cdot 10^{-5}$	$1.2 \cdot 10^{-4}$	$1.8 \cdot 10^{-4}$	$1.2 \cdot 10^{-4}$
21	$6.0 \cdot 10^{-5}$	$1.4 \cdot 10^{-4}$	$2.0 \cdot 10^{-4}$	$1.3 \cdot 10^{-4}$

Table 14
Case 4: Failure probability for a weather-unrestricted operation based on data for January and year-round wave data.

No. of days	P_f	
	Jan.	Year-round
3	$1.6 \cdot 10^{-4}$	$6.1 \cdot 10^{-5}$
7	$2.2 \cdot 10^{-4}$	$8.5 \cdot 10^{-5}$
14	$2.8 \cdot 10^{-4}$	$1.1 \cdot 10^{-4}$
21	$3.2 \cdot 10^{-4}$	$1.3 \cdot 10^{-4}$

3.4. Case 3: The influence of the startup date within a season

For the case in Section 3.3, we study how the startup date within the season (i.e., the month within a season in which the operation is executed) affects the failure probability.

Let us use the statistics for the autumn—i.e., September–November. The failure probabilities based on the monthly and seasonal statistics from Tables 7 and 8 are shown in Table 13. The failure probability is 1.5 times higher if the analysis is based on data from November instead of seasonal data. If the analysis is based on data for September, P_f is less than half that calculated for the season.

3.5. Case 4: The effect of seasonal versus year-round data

ISO 19901-6 (2009) requires that the weather conditions used for the design of weather-unrestricted operations "shall reflect the statistical extremes for the area and season concerned". According to DNVGL-ST-N001 (2020), seasons *may* be accounted for when planning sea voyages.

We now discuss the effect of using seasonal or monthly versus year-round statistics. Traditionally, the use of seasonal variations has been optional. The normal approach has generally been to use year-round data and utilize seasonal variations when it is beneficial in the sense that the loads are reduced.

We again consider the weather-unrestricted seafastening design from Section 3.1.2. In Table 14, P_f is calculated based on environmental data from January and year-round data. The failure probability is 2–3 times higher based on January statistics than on year-round data. Next, let us assume a duration equal to seven days, for example. We compare P_f for each month with that calculated with year-round data. The P_f based on year-round data is $8.5 \cdot 10^{-5}$, while P_f based on monthly data varies, as shown in Fig. 7. For operations during the summer period, P_f is very low, as expected. This could be viewed as (unnecessary) conservatism by the use of the weather-unrestricted design option for the summer period. If the seafastening system is designed based on year-round data and transport is performed in January, the failure probability is three times the target level.

As mentioned in Section 2.7 , the duration of a marine operation is actually a stochastic variable that has been assumed to be a deterministic variable in the structural reliability analysis. The duration could be modeled as a stochastic variable, and the revised failure probabilities could be calculated. However, from the case studies above, it is observed that P_f is not very sensitive to the duration, so it is reasonable to model the duration as a fixed variable.

Table 15
Importance factors (in %) for weather-restricted (WR) and weather-unrestricted (UR) operations with durations of three and seven days, respectively. The reliability index and failure probability are also given. Index 0: Base case with variables from Table 4. Index 1: Alternative 1 with the bias for χ_R changed from 1.25 to 1.15. Index 2: Alternative 2 with the COV for $\chi_{S,E}$ changed from 0.14 to 0.20. Index 3: Alternative 3 with the COV for χ_R changed from 0.17 to 0.15. Index 4: Alternative 4 with the COV for χ_R changed from 0.17 to 0.20.

			Importance factors, %			
Case	β	P_f	χ_R	$\chi_{S,E}$	S_e	$\chi_{S,G}$
WR-0	3.21	$6.6 \cdot 10^{-4}$	77	7	8	8
WR-1	2.78	$2.7 \cdot 10^{-3}$	76	7	8	8
WR-2	3.10	$9.5 \cdot 10^{-4}$	72	13	9	7
WR-3	3.54	$2.0 \cdot 10^{-4}$	72	9	10	9
WR-4	2.81	$2.5 \cdot 10^{-3}$	82	6	6	6
UR-0	3.76	$8.5 \cdot 10^{-5}$	60	8	27	4
UR-1	3.38	$3.6 \cdot 10^{-4}$	59	8	29	5
UR-2	3.63	$1.4 \cdot 10^{-4}$	55	14	28	4
UR-3	4.05	$2.5 \cdot 10^{-5}$	57	10	29	5
UR-4	3.38	$3.6 \cdot 10^{-4}$	65	6	25	4

3.6. Sensitivity study

The importance factors (see Section 2.6.2) for two selected cases, one weather-restricted and one weather-unrestricted, are shown in Table 15. In the weather-restricted case, the seafastening system is designed for a significant wave height equal to 4 m, and the operational duration is three days (72 h). The forecasted H_s is 2.7 m (from Table 3). In the weather-unrestricted case, the duration is seven days, and the significant wave height is based on year-round long-term statistics. The vertical support was designed for weather-unrestricted transport (see Section 3.1.2).

In addition to the base cases, we consider alternatives with changes in bias and COV on the capacity and one alternative with increased COV on the uncertainty in the calculated dynamic load effect. Details on the alternatives and the importance factors, as well as the reliability index and the failure probability, are given in Table 15. The importance factor for the structural capacity, χ_R, dominates in all cases. For weather-unrestricted operation, the wave-induced load, S_E, contributes significantly more to the failure probability than for weather-restricted operation. As expected, the failure probability increases when the bias on χ_R is reduced and when the COV of $\chi_{S,E}$ is increased. In Alternative 4, an increase in the COV for the capacity leads to a substantial increase in the failure probability. The main observation is that the uncertainty in the structural capacity dominates in the structural reliability analyses. The capacity depends on the structural design and fabrication for actual transport, and a focus on this aspect is suggested in the planning of grillage and seafastening in connection with the transport of heavy objects.

4. Results and discussion

This paper analyzes the implied failure probability of a seafastening structure designed by the use of standard motion criteria for a barge transport operation, incorporating the influence of weather forecasts, the duration of the transport and the time of year. Two categories of marine operations have been considered, i.e., weather-restricted and weather-unrestricted operations. In the first category, the significant wave height is given by weather forecasts, and the uncertainty in the forecasts is accounted for. In the second category, the significant wave height is based on long-term statistics regarding the northern North Sea.

The motion analysis of the transport barge is limited to situations with wind-generated seas acting in one main direction. In our case, rolling of the barge dominates the loading, and the load effects in the supports are overestimated. More realistic modeling would include wind-generated sea and swell with different mean directions. Such an extension of the analysis would require a more detailed assessment of the model uncertainty related to such conditions than is included in the present analysis but may be interesting to include in future studies.

The sensitivity analyses show that the structural capacity has the largest importance factors of the parameters examined (Table 15). Consequently, the failure probabilities are sensitive to variations in the bias and COV for the structural capacity. The structural capacity of a bulkhead with horizontal stiffeners exposed to vertical loading should be studied, for example, by a more detailed load effect calculation and detailed FE-analyses of the support points, to reduce the uncertainty in this variable.

For a *weather-restricted* operation, the failure probabilities are calculated by the following two methods—i.e., by assuming that the decision to start sea transport is made:

- accounting for the uncertainty in the weather forecasts and
- not accounting for the uncertainty in the weather forecasts (i.e., assuming perfect forecasts).

The reduction in the maximum allowed significant wave height in the Alpha factor method compensates for the forecast uncertainty such that P_f is lower when the forecast uncertainty is included than when it is not (see Table 10). The failure probabilities shown in Table 10 are sensitive to the input parameters, and they are somewhat higher than 10^{-4} per operation. However, the comparison of the probabilities, not the absolute values, is of main interest here.

The failure probability for a *weather-unrestricted* operation depends on the time of year the operation is executed. For example, case studies indicate that for a given seafastening design,

- the failure probability is 1.5 times higher using environmental data for November instead of seasonal data for the autumn (September–November),
- the failure probability calculated using statistical data for January is three times higher than that calculated using year-round data, and
- the failure probability is 15–20 times higher in October than in July for a design based on standard motion criteria.

The differences in the failure probabilities are not dramatic in the first two examples; a consequence of the first bullet point is that a marine operation executed in November may be designed based on seasonal data for the autumn and not necessarily the actual month. Furthermore, an operation executed in January designed for year-round data will have a failure probability equal to three times the target value, which is still not dramatic. In the third bullet point, it is assumed that the standard weather-unrestricted criterion has been applied for the design of the grillage and seafastening. While the failure probability is equal to the target level for October transport, this probability is much lower for summer transport, introducing additional conservatism. Conservatism is acceptable but results in an increased fabrication cost. An alternative to an unrestricted design could be to estimate the design sea state for the geographic area, time of year and duration of the operation

and to design the grillage and seafastening for that sea state—e.g., the $H_s = 6$ m or $H_s = 4$ m criterion in DNVGL-ST-N001 (2020) for weather-unrestricted transport operations.

5. Conclusions and recommendations

Based on the study, the following conclusions are drawn:

- For a weather-restricted operation, the reduction in the wave height to account for the forecast uncertainty compensates adequately for the uncertainty inherent in the forecasted significant wave height and is a good approach with respect to the failure probability.
- For weather-unrestricted transport, the use of seasonal or annual data affects the results. The use of seasonal data is optional in DNVGL-ST-N001 (2020), where seasonal data "may" be accounted for. The use of seasons could also be mandatory, e.g., as required by ISO 19901-6 (2009), which requires that the statistical extremes for the season concerned be reflected. It is recommended that this aspect be considered for inclusion in future design standards.
- The calculated failure probabilities in the study span a large range as a result of seasonal variations. However, the calculated probabilities are of the same order of magnitude as the target value indicated by DNVGL-ST-N001, of 10^{-4} per operation.

For the North Sea, the failure probability obtained by using the simplified design criteria compares well with the target reliability level. However, because the uncertainty in strength dominates and the strength depends on temporary solutions for each transport operation, a focus on this aspect is recommended in the integrity management of the grillage and seafastening in connection with transport of heavy objects.

In the present work, the design of the module supports is based on motion from a design standard. It would be of interest for future work to study the reliability level of a transport designed according to criteria from other design standards or by vessel motions obtained from the 3D panel model. The effect of wind seas and swell with different mean directions is also of interest for future work.

CRediT authorship contribution statement

Asle Natskår: Responsible for initiating the ideas, Performing the analysis and calculations, Providing the results, Writing the paper. **Torgeir Moan:** Providing support, corrections and constructive comments to increase the scientific quality of the paper.

Declaration of competing interest

The authors declare that they have no known competing financial interests or personal relationships that could have appeared to influence the work reported in this paper.

Acknowledgments

The first author has received financial support from the Research Council of Norway (RCN) through the Center for Ships and Ocean Structures (CeSOS) at the Norwegian University of Science and Technology (NTNU) , as well as support from DNV through Det Norske Veritas' Education Fund. The support is greatly appreciated. RCN and DNV had no active roles in the research work. Hindcast data were obtained from Magnar Reistad at the Norwegian Meteorological Institute and are also greatly appreciated. The first author is grateful to Per Ø. Alvær, Øistein Hagen, Gudfinnur Sigurdsson and Gunnar Solland at DNV for their discussions, support and inspiration. Thank you to the reviewers for their valuable comments helping us to improve the quality of the paper.

References

Bitner-Gregersen, E., Haver, S, 1991. Joint environmental model for reliability calculations. In: ISOPE. Proc. 1st Int. Offshore and Polar Eng. Conf., Edinburgh, UK, pp. 246–253.

Brooker, D.C., Cole, G.K., McConochie, J.D., 2004. The influence of hindcast modeling uncertainty on the prediction of high return period wave conditions. In: Proceedings of the 23th International Conference on Offshore Mechanics and Arctic Engineering, OMAE, Vancouver, British Columbia, Canada.

Bruserud, K., Haver, S., 2016. Comparison of wave and current measurements to NORA10 and NoNoCur hindcast data in the northern North Sea. Ocean Dyn. 66, 823–838. http://dx.doi.org/10.1007/s10236-016-0953-z.

Bury, K.V., 1999. Statistical Distributions in Engineering. Cambridge University Press.

De Girolamo, P, Di Risio, M, Beltrami, G., Bellotti, G., Pasquali, D., 2017. The use of wave forecasts for maritime activities safety assessment. Appl. Ocean Res. 62, 18–26. http://dx.doi.org/10.1016/j.apor.2016.11.006.

DNV-RP-C201, 2010. Buckling Strength of Plated Structures. Det Norske Veritas, Oslo, Norway.

DNVGL-OS-C401, 2019. Fabrication and Testing of Offshore Structures. DNV GL, Oslo, Norway.

DNVGL-ST-N001, 2020. Marine Operations and Marine Warranty. DNV GL, Oslo, Norway.

EN 1990, 2005. Eurocode: Basis of Structural Design. European Committee for Standardization, Brussels, Belgium.

EN 1993-1-1, 2005. Eurocode 3: Design of Steel Structures - Part 1-1: General Rules and Rules for Buildings. European Committee for Standardization, Brussels, Belgium.

Gintautas, T., Sørensen, JD, 2016. Evaluating a novel approach to Reliability based decision support for offshore wind turbine installation. In: RENEW 2016, Lisbon, Portugal.

Guachamin Acero, W., Moan, T., Gao, Z., 2015. Steady state motion analysis of an offshore wind turbine transition piece during installation based on outcrossing of the motion limit state. Proceedings of the ASME 34th International Conference on Ocean and Arctic Engineering, OMAE, St. John's, NL, Canada.

Guachamin Acero, L., Gao, Z., Moan, T, 2016. Methodology for assessment of the operational limits and operability of marine operations. Ocean Eng. 125, 308–327.

Haakenstad, H., Breivik, O., Reistad, M., Aarnes, O.J., 2020. NORA10EI: a revised regional atmosphere-wave hindcast for the north Sea, the Norwegian Sea and the Sarents Sea. Int. J. Climatol. 40, 4347–4373. http://dx.doi.org/10.1002/joc.6458.

Haver, S, 1994. Uncertainties Related to Hindcast Wave Data. Proceedings of the 13th International Conference on Offshore Mechanics and Arctic Engineering, OMAE, Houston, Texas, USA.

ISO 19901-6, 2009. Petroleum and Natural Gas Industries. Specific Requirements for Offshore Structures. Part 6: Marine Operations. International Organization for Standardization, Geneva, Switzerland.

ISO 2394, 2015. General Principles on Reliability for Structures. International Organization for Standardization, Geneva, Switzerland.

JCSS, 2000. Probabilistic model code. Part 3: Material properties. Joint Committee on Structural Safety (JCSS). https://www.jcss-lc.org.

Madsen, H, 1988. Omission sensitivity factors. Struct. Saf. 5, 35–45.

Madsen, H., Krenk, S., Lind, N., 1986. Methods of Structural Safety. Prentice-Hall Inc. Englewood Cliffs, New Jersey, USA.

Melchers, R.E., Beck, A.T., 2018. Structural Reliability Analysis and Prediction. Third Ed.. John Wiley & Sons Ltd, Hoboken, New Jersey, USA.

Moan, T., 1995. Safety Level Across Different Types of Structural Forms and Materials - Implicit in Codes for Offshore Structures. Technical Report. SINTEF Report No. STF70 A95210. Trondheim, Norway.

Moan, T., Gao, Z., Ayala-Uraga, E, 2005. Uncertainty of wave-induced response of marine structures due to long-term variation of extratropical wave conditions. Mar. Struct. 18, 359–382.

Naess, A., Moan, T., 2013. Stochastic Dynamics of Marine Structures. Cambridge University Press, New York, USA.

Natskår, A., Moan, T., Alvær, P.Ø, 2015. Uncertainty in forecasted environmental conditions for reliability analyses of marine operations. Ocean Eng. 108, 636–647.

Natskår, A., Steen, S., 2013. Rolling of a transport barge in irregular seas, a comparison of motion analyses and model tests. Marine Syst. Ocean Technol. 8, 5–19.

Rajashekhar, M.R., Ellingwood, B.R., 1993. A new look at the response surface approach for reliability analysi. Struct. Saf. 12, 205–220.

Reistad, M., Breivik, Ø, Haakenstad, H., Aarnes, O.J., Furevik, B.R., Bidlot, J., 2011. A high-resolution hindcast of wind and waves for the North Sea, the Norwegian Sea, and the Barents Sea. J. Geophys. Res. 116, 18.

SESAM, 2019. Software Suite for Hydrodynamic and Structural Analysis of Ships and Offshore Structures, Feature Description. DNV GL, Oslo, Norway.

Shu, Z., Moan, T, 2011. Reliability analysis of a bulk carrier in ultimate limit state under combined global and local loads in the hogging and alternate hold loading condition. Mar. Struct. 24, 1–22.

SSC-433, 2004. Interactive buckling testing of stiffened steel plate panels. Technical Report, Ship Structure Committee, Washington D.C., USA.

Tvedt, L., 2006. Proban - probabilistic analysis. Struct. Saf. 28, 150–163.